processes

MDPI

Article

Pressure Source Model of the Production Process of Natural Gas from Unconventional Reservoirs

Boubacar Yarnangoré and Francisco Andrés Acosta-González *

Centro de Investigación y de Estudios Avanzados del Instituto Politécnico Nacional, Unidad Saltillo, Av. Industria Metalúrgica # 1062, Industrial Park "Saltillo-Ramos Arizpe", Ramos Arizpe 25900, Mexico; boubacar.yarnangore@cinvestav.mx

* Correspondence: andres.acosta@cinvestav.edu.mx

Abstract: This work is focused on developing a computational model to predict the production rate and pressure evolution of natural gas from unconventional reservoirs, particularly shale gas deposits. The model is based on the principle of conservation of mechanical energy and was developed from the transient solution of Bernoulli's equation. This solution was obtained by computing the pressure evolution in the well resulting from the combined action of extracting the free gas and of gasification from kerogen. The transient behavior of gas production by hydraulic fracturing was calculated by numerically integrating Bernoulli's equation. The curves representing gas flow evolution were considered as a series of stepwise steady states under a constant gas flow rate, similar to the pressure–time curves. These time steps were connected by instantaneous drops in pressure or gas flow rates. On the other hand, the delayed release of the adsorbed and dissolved gas in the kerogen was accurately calculated by introducing a semi-empirical gas pressure source term into the gas well pressure equation. The effect of this source is to gradually increase the gas pressure in the reservoir, emulating the gas release mechanisms from the organic matter. Model validation was based on production data from the unconventional reservoirs Eagle Ford, U.S.A., and Burgos basin, México. The initial measured gas production rate was used to determine a global friction factor of the gas flowing out from soil cracks and ducts. Additionally, measured production rate data were used to determine the coefficients of the source term function. Pearson correlation coefficients of 0.97 and 0.96 were obtained for Eagle Ford and Burgos basins data, respectively. In contrast, the corresponding coefficients calculated from the traditional Arps' model were 0.89 and 0.5, respectively. The present pressure source model (PSM) represents a new approach to characterize the process of gas production from unconventional reservoirs, proving to be accurate in forecasting both the gas flow rate and pressure evolution during gas production. The postulated pressure source term was shown to mimic the desorption and diffusion kinetics, which release free gas from the kerogen.

Keywords: shale gas; hydraulic fracturing; unconventional gas deposit; Bernoulli's equation; gas in kerogen; free natural gas; pressure source

Citation: Yarnangoré, B.; Acosta-González, F.A. Pressure Source Model of the Production Process of Natural Gas from Unconventional Reservoirs. *Processes* **2024**, *12*, 1875. https://doi.org/10.3390/pr12091875

Academic Editor: Zheng Sun

Received: 15 June 2024
Revised: 21 August 2024
Accepted: 23 August 2024
Published: 2 September 2024

1. Introduction

Natural gas is a mixture mainly consisting of methane (~95% volume), ethane (~4% volume), and smaller proportions of other hydrocarbons, nitrogen, and carbon dioxide. Therefore, we will refer simply to methane or hydrocarbons as synonyms of natural gas. Unconventional reservoirs of natural gas have become a very important alternative to obtaining fossil energy in the United States. Other countries such as China, Canada, and Australia are currently investigating the potential of this promising resource. Unconventional reservoirs include several types of deposits: shale gas, tight gas sandstone, coalbed methane, and methane hydrates. This work aimed to study shale gas, which represents a large and growing share of the U.S.'s recoverable resources.

Unlike conventional gas reservoirs where methane is accumulated in underground voids and caverns, the distribution of methane in shale gas deposits is complex. The

methane distributes in three sites: (1) free gas stored in the network of cracks and intergranular porosities in the shale, which is a very fine-grained sedimentary rock; (2) dissolved methane, which is distributed in the organic phase, called kerogen or bitumen, and is in turn distributed within the shale; and (3) adsorbed methane, located on the surface of micropores with a pore diameter (dp) < 2 nm and mesopores ($2 \leq dp \leq 50$ nm) formed in the organic matter. Etminan et al. [1] carried out a laboratory study of the gas storage distribution in shale and determined the diffusion coefficient of methane in kerogen. The authors developed the batch pressure decay (BPD) technique to measure the gas volume stored in each one of the above-mentioned three sites in a single experiment. They used thin disks (~7 g) from a shale-core plug sample. The authors identified that at an early stage, ~4 min, free gas came out initially. Then, gas desorption from the organic pores followed at around ~2:30 h, and finally, gas diffusion from the organic material was detected until the end of the test, ~100 h. A mass balance was used to determine the gas proportion released from each site. Free gas and adsorbed gas contributed almost equally, 38% each, to the total gas-in-place, while dissolved gas was about 22% of the total gas-in-place. The rate of release of dissolved methane was controlled by a low diffusion coefficient, which the authors reported to be on the order of 10^{-20} m^2/s. Chalmers et al. [2] characterized the shale-gas pores by measuring the total porosity, pore-size distribution, surface area, organic geochemistry, mineralogy, and image analysis by field emission scanning electron microscopy/transmission electron microscopy, using samples prepared with focused ion beam milling (FIB). The authors analyzed samples form Barnett, Marcellus, Woodford, and Haynesville gas shales in the U.S. and the Doig Formation in northeastern British Columbia, Canada. They showed the nature and variability in pore structures within gas shales. They found that aggregates of kerogen, clay and/or carbonate contain mostly macropores (dp > 50 nm) and mesopores in the studied samples and that those samples with greater pore interconnectedness would show improved access to the surface area of the mesopores and micropores within the organic matter, enhancing the matrix permeability of the reservoir. Curtis [3] presented a review of five principal shale-gas exploited systems in the U.S.: Antrim, Ohio, New Albany, Barnett, and Lewis shale basins. He showed some well data including the adsorbed gas content for these basins, which is between 20% (Barnett Basin) and 85% (Lewis Basin). Furthermore, all these gas reservoirs exhibit wide ranges of geological and geochemical parameters that affect the proportion of adsorbed gas. Therefore, gas flow rate production will depend not only on well stimulation treatments (fracking) but also on the thermal history of organic matter and the response of the shale matrix and organic matter to local and global stresses. For the previous reasons, it is important to develop models for predicting the rate of gas release from unconventional gas deposits.

Fathi and Akkutlu [4] developed a gas transport model to investigate the effect of local spatial heterogeneities in porosity and the material content of the matrix on the rate of gas production from a laboratory-size sample. The free gas flow, diffusive transport, and adsorption/desorption rates were introduced in their model to carry out a perturbation analysis. The authors adopted weak-noise and mean-field approximations and used a statistical approach in spectral domain to find that the matrix heterogeneities generate non-trivial, macro-transport, and macro-kinetics effects on the system that retard gas release from the matrix and adversely influence the gas recovery. No measured data were used to validate the model results.

Nobakht et al. [5] developed a simplified method of production forecasting for tight/shale-gas reservoirs showing an initial period of linear gas flow. The method is applicable to hydraulically fractured vertical wells and multi-fractured horizontal wells leading to isobaric gas flow. This model combines the theory of linear flow with hyperbolic decline during boundary-dominated flow. The authors claimed that the model does not require superposition time functions nor pseudo time. The only required major well parameter is the drainage area, which unfortunately is the parameter with the greatest uncertainty, particularly in the first year of gas production. Model validation was carried out using Marcellus and Barnett shale gas production data. Javadpour et al. [6] presented a

review on the gas flow models of shale. The authors pointed out that conventional flow models based on Darcy's law cannot model shale gas production accurately, even after including molecular dynamics or lattice Boltzmann methods. This failure to match field data and laboratory-scale results has been attributed to the complexity of multi-scale pore size in shales. On the one hand, nanopores are present in the organic matter. The size of these pores is from a few to hundreds of nanometers. On the other hand, micropores are present in the inorganic matter and are generally on the order of microns, much larger than the organic nanopores. The authors found that pore network models have been used extensively by many researchers to upscale nanoscale gas flow from a single nanopore to a network of interconnected nanopores. However, most efforts have focused on modeling the microscale behavior of gas, while few models have been aimed on the scale-up calculation. The authors concluded that more research is needed to apply shale permeability models to field scale. Arevalo et al. [7] performed a dynamic characterization of unconventional gas reservoirs where gas production could be estimated from two unconventional reservoir wells: Eagle Ford formation in Texas, and northeastern wells in Mexico. They concluded that Langmuir's isotherm model is appropriate to predict the behavior of adsorbed and desorbed gas in unconventional formations that contain organic material. The authors pointed out that this result is important since, once gas desorption pressure is reached, there is an additional production mechanism of gas. Song et al. [8] used the fractal theory to calculate the gas slippage factor in porous media considering both gas adsorption and no gas adsorption. The slippage factor is important for determining the apparent gas permeability of the porous medium. Two important model parameters that are required are the pore fractal dimension and tortuosity fractal dimension. The model predictions are in good agreement with molecular simulation and experimental data from other researchers. The authors conclude that the gas slippage factor depends on the structural parameters of porous medium, adsorption capacity, reservoir properties, and gas properties. Li et al. [9] developed a simulation model to predict the production rate of a refracturing shale gas well. The model is based on the coupled solution of the equations for fluid flow and geomechanics in triple continuum media including kerogen, gas, and an inorganic matrix. A fracture network is proposed considering the multiscale flow characteristics of shale gas, the induced stress of fracture opening, and the pore elastic effect. A sensitivity analysis is performed to study the effects of the refracturing pattern, fracture conductivity, width of the stimulated reservoir volume (SRV), SRV length of new and initial fractures, and refracturing time on the production increase percentage (PIP). Younk [10] applied the hyperbolic decline curve analysis method to data from the Bakken and Barnett formations. The coefficients of the non-linear regression equation were obtained for the most recent 5 years of data. The author presents some analysis guidelines to obtain satisfactory long-term predictions. Another recent effort to predict shale gas production and to optimize horizontal well parameters was reported by Wang et al. [11], who developed a model based on machine learning to optimize multistage fractured horizontal wells. They combined Gaussian Process Regression (GPR) and Convolution Neural Network (CNN) to complement a numerical simulation model and achieve rapid optimization. Their sensitivity analysis identified porosity, permeability, fracture half-length, and horizontal well length as influencing factors. Furthermore, the n-factorial experimental design was applied to design the initial experiment, and the dataset was constructed by combining the simulation results with the case parameters. The authors reported that well parameter optimization using GPR was carried out in 1/720 of that period for numerical simulation. However, no details were described regarding the simulation model itself.

Laboratory experiments consistently confirm that natural gas is distributed as free gas in pores and cracks, adsorbed gas on the surface of nanopores, and dissolved gas in the kerogen, and these experiments also identify the role of production pressure on gas extraction. Sang et al. [12] presented laboratory results for tests using four shale gas core samples from a shale gas reservoir in China and one sample from a tight sandstone reservoir in Canada. The authors found that the contributions of free gas, adsorbed gas, and

dissolved gas to the cumulative gas production were affected by the production pressure. They reported a critical production pressure at which shale gas can be efficiently desorbed and diffused from kerogen. At high production pressures, the adsorbed gas extraction is mainly affected by the shale desorption properties, while at low pressures, the adsorbed gas extraction is affected by the stress sensitivity of permeability. These results show the importance of considering the production pressure for proper gas extraction modeling. Well pressure is a process variable that has been remarkably missed in most empirical models for gas production prediction.

The most accepted and widely used fundamental approach to predict the rate of gas production is based on Darcy's law, which is given by the following expression:

$$W = \frac{\rho k A}{\mu} \frac{\Delta p}{L}, \quad (1)$$

where W is the fluid mass flow rate (kg/s), ρ is the average gas density (kg/m^3), k is the permeability (m^2), A is the cross-sectional area (m^2), μ is the fluid viscosity (Pa s), and Δp is the pressure difference (Pa) between two points separated by a distance L (m) that is measured along the flow direction. The permeability is a property of porous media that represents the ease with which a fluid flows through these media when a pressure gradient is applied. Singh and Cai [13] presented a critical discussion of papers on the permeability of fractured shale and also presented a summary of their previous work on brine-gas relative permeability in fractures. The authors included experimental and modeling results aimed to understand gas transport processes in shale that determine the permeability at different times during the well's lifespan. They explained that experimental work has been focused on characterizing permeability using steady-state or unsteady-state laboratory methods. From these measurements, the permeability of laboratory samples can be studied as a function of other variables, such as the pore diameter, pore porosity, gas pressure, residual brine saturation, etc. On the other hand, shale permeability models have been developed considering the complex characteristics of shale-gas systems, namely, (1) gas rarefaction in pores and cracks during gas extraction, which leads to correction formulae specified as a function of the Knudsen dimensionless number (Kn = λ/L, λ = mean free path of gas molecules, L = representative physical length scale); (2) the compressibility of the gas, shale matrix and shale bulk; (3) the kinetics of gas adsorption–desorption on pore and crack surfaces; (4) stress, strain, and damage of cracks; (5) local heterogeneity; (6) the imbibition of slick frack water into the matrix by osmosis (counter-imbibition); and (7) gas dissolved in organic matter. The parameters of these permeability models can be determined from laboratory tests of core samples. On the other hand, the determination of field-scale permeability requires a further method; for example, for unconventional reservoirs, history-matching has been used successfully. It consists of estimating the parameters included in the permeability models by minimizing the difference between the computed and the measured gas production rates. Therefore, using historical production data is possible to determine a more accurate forecast for the field-scale permeability. Another method that has been used traditionally for conventional reservoirs is the well logs (measurements of properties, e.g., density and hydrogen index). In this case, the permeability is determined using mathematical relationships between permeability and the well logs. These relationships can be obtained from either empirical data from core samples or well-known porous media models, for example, the Blake–Kozeny model. Application of well logs to unconventional reservoirs is questionable for two reasons: (i) the shale properties do not represent a statistically significant correlation with permeability, and (ii) kerogen exhibits log responses that are indistinguishable from pore fluid, causing the logging tools to read excessively high or low values. Finally, the authors present a summary of their formulation of the two-phase relative permeability in shale fractures. Their work also models the upscaled permeability by accounting for distinct ground characteristics using a finite difference grid that contains fractures and matrix.

Some selected examples of permeability models developed for shale matrix are the following. Darabi et al. [14] studied the gas flow process in ultra-tight porous media that included nanometer- to micrometer-size pores. They formulated a pressure-dependent permeability function assuming Knudsen diffusion and slip flow (the Klinkenberg effect). Slip flow occurs when $0.001 < Kn < 0.1$, which represents moderate gas rarefaction, but Knudsen diffusion corresponds to ultra-rarefaction levels, $Kn > 10$. The model predicts that in nanometer-size pores, the gas permeability values are as much as 10 times greater than the results obtained by continuum hydrodynamics predictions ($Kn < 0.001$). However, with increasing pore size (i.e., on the order of micrometers), the gas permeability converges to continuum hydrodynamics values. The authors used the pulse-decay laboratory method (an unsteady-state technique) to estimate the main parameter of the model, which is the Darcy permeability.

Civan [15] developed a correlation of apparent gas permeability in tight porous media. His model is based in a unified Hagen–Poiseuille-type equation representing the porous media as a bundle of tangled tubes and includes parameters such as the intrinsic permeability, porosity, tortuosity of the apparent gas permeability, rarefaction coefficient, and Klinkenberg gas slippage factor. His formulation was used to obtain an improved correlation of available laboratory data with respect to previous models.

Cao et al. [16] developed a fully multiscale shale deformation–gas transport model. Their model consisted of the solution of a set of partial differential equations to calculate the following processes: (1) the mechanical equilibrium equation that defines the shale body deformation; (2) gas flow in the kerogen system of matrix; (3) gas flow in the inorganic system of matrix; and (4) gas flow in the hydraulic fracture system. For each gas flow system, a permeability or diffusivity model was derived to define its evolution. The verified model was applied to investigate the impact of the adsorption parameters, flow regimes (defined by the Knudsen number), the initial permeability of the inorganic matrix, and the effective stress variations on the gas production rate. Model predictions were compared with the respective production rates in the Marcellus and Barnett shales, in the U.S.

Yuan et al. [17] presented an analytical model of apparent gas permeability for tight porous media. Their approach also considers a porous medium as equivalent to a bundle of tangled tubes. However, the distribution of capillary diameter and tortuosity were computed using fractal theory. The authors studied the effect of pore size distribution, fractal dimensions for pore size and tortuosity, porosity, surface diffusivity, and Langmuir parameters on flow rate processes in tight rocks.

Sheng et al. [18] also used fractal theory to consider the effect of multi-scale pore spaces on shale-gas permeability. The authors considered various flow regimes that occur in these multi-scale pores. They confirmed that gas permeability varies with the pore-size distribution of the samples, even when they have the same intrinsic permeability value.

Yang et al. [19] developed a model of Dynamic Adsorption–Diffusion (DAD) to represent gas transport and storage in crushed shale at three different particle sizes. The mathematical model for this phenomenon was validated on dynamic adsorption experiments with a constant pressure condition. It was found that the absolute permeability decreases with crushing to smaller particles. Furthermore, particle size plays a more important role on diffusion than on permeability.

All the above mathematical models have been focused on predicting the evolution of flow of gas released mainly from a laboratory sample or in some cases from an unconventional reservoir. To the best of our knowledge, very few reports include pressure evolution in the reservoir. It should be clear that both the gas flow rate and pressure evolve during well production. Moreover, pressure cannot be dependent only on the amount of recovered gas but also on the amount of gas that is being released from the kerogen. Recently, Gu et al. [20] reported a study of the gas pressure field and production rate when using proppants with two different particle sizes. They solved the mass conservation equation for gas and water phases and the corresponding Darcy's equations for them. They

found that using proppants with a larger particle size will lead to a lower permeability and therefore to larger gas production rates.

In this paper, we propose a completely new model that introduces a semi-empirical pressure source equation representing the gasification kinetics from the kerogen. The model is based on the transient solution of the conservation of mechanical energy equation (Bernoulli's equation) and the conservation of gas mass (continuity equation) to predict the evolution of gas flow and pressure in an unconventional reservoir. This approach is more computationally efficient than those based on the numerical solution of the conservation of mass and momentum differential equations. Moreover, it is consistent with previous models based on Darcy's equation and the Langmuir desorption model. Actual production data from unconventional natural gas wells were used for model validation.

2. Materials and Methods

2.1. Mathematical Formulation

This section describes the mathematical formulation of the model. First, the considered system is defined. Then, the transient solution of Bernoulli's equation is presented, together with the assumptions of the system. The input and output variables are defined. Finally, the solution method is described.

2.1.1. Modeling System

We analyzed the gas production of unconventional wells. These wells are in the United States and Mexico, and their characteristics are described as follows [7]:

- Well "A", Eagle Ford: It is a well that is in the shale of the Eagle Ford formation in southern Texas. It is a horizontal dry gas producing well, which was completed with a stimulation treatment of ten stages of lateral fracturing. The well has carried approximately 20 effective transverse fractures.
- Well "B", Burgos basin: It is in northern Mexico and was drilled and completed in February 2011 with horizontal geometry in the Upper Cretaceous Eagle Ford formation. The well has carried approximately 17 effective fractures.

The characteristics of both wells and their initial conditions are presented in Table 1. Gas temperature values are shown in both K and °C and correspond to the gas in place underground. Manometric pressure is the difference between the absolute pressure (location 1 is underground) and barometric pressure (location 2 is ground level). Index "0" indicates initial time, t = 0.

Table 1. Characteristic data of wells "A" and "B" [7].

Variables	Well 'A'	Well 'B'
Depth of well, Δz (m)	3048	2600
Temperature of gas in the well, T_1 (K) [°C]	(414) [141]	(370) [97]
Initial manometric gas pressure in the well, ${p_1}^0 - p_2$ (MPa)	25	18.5
Cross-sectional area of the extraction duct, A_d (m^2)	0.032	0.040
Production period (h)	6000	2800

Figure 1a shows the measured data points together with smoothed out curves for the gas production flow rate and pressure drop during the first 9 production months for well "A" [7]. A locally weighted scatter plot smooth method ("loess") was used to smooth out the original dispersed data. The pressure drop is the instantaneous manometric gas pressure at the bottom of the well ($\Delta p = p_1 - p_2$). The initial manometric pressure at the bottom of well "A" was 25 MPa, which drove an initial gas flow rate of 8.9 Nm^3/s. The production flow rates are given in normal m^3/s, that is, at 0 °C and 1 atm pressure. Gas pressure decreased with time during gas extraction up to a final value of 9.3 MPa, with a gas volume flow of 2.1 Nm^3/s. It should be noted that these curves are the net result of releasing methane that was naturally stored in the three locations previously described (in

cracks as free gas, in the surface area of pores as adsorbed methane, and in organic matter as dissolved methane). The changes in the production rate slope reflect a sequence during gas extraction. The gas located in the cracks releases rapidly in a time less than 400 h. The adsorbed gas starts to release from that time, and finally, the gas dissolved in the kerogen begins to release after 5600 h.

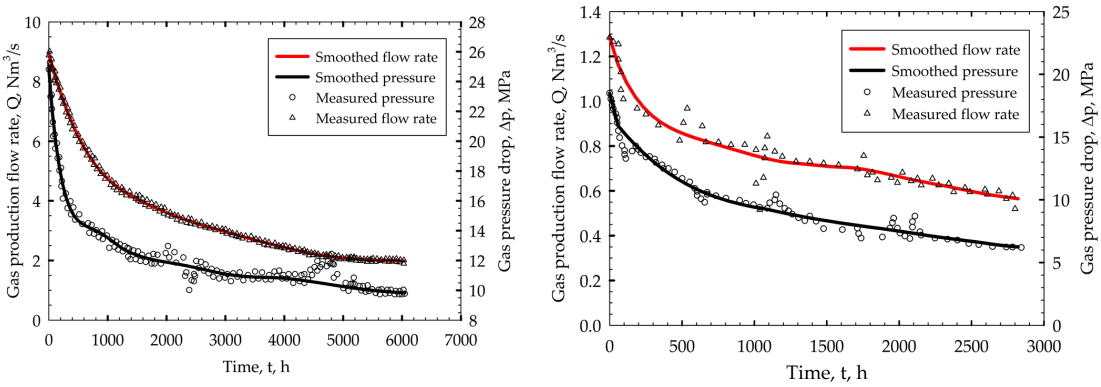

Figure 1. Measured gas production flow rate and pressure drop and the corresponding smoothed curves for wells (**a**) "A" and (**b**) "B". Data points from Ref. [7].

Figure 1b shows the corresponding curves for well "B" during 4 months of gas production [7]. The manometric gas pressure started at 18.5 MPa and dropped to a final pressure of 6.2 MPa. The initial gas flow rate was 1.3 Nm^3/s and decreased to 0.6 Nm^3/s. Free gas released rapidly in a time of less than 100 h, and adsorbed gas followed thereafter. Finally, dissolved gas began to release after 2600 h.

It is convenient to notice that in contrast with most of the laboratory experiments where samples are subjected to a constant pressure during the process of gas releasing, in actual wells, the gas pressure at the bottom of the well varies as a function of time.

Figure 2a shows a schematic representation of these wells. Points 1, 2′, and 2 correspond to specific control positions considered in our model. Point 1 represents all the tips of the produced fractures by hydraulic cracking. These positions are the starting points for the gas to flow to the ground surface. Point 2 is the well exit, the point where the gas is collected, and point 2′ is an intermediate position in which gas expansion switches from adiabatic expansion to isothermal expansion. This is explained in detail in Section 2.1.2. Figure 2b is a simplified representation of the well, indicating the control points 1, 2′, and 2. Bernoulli's equation was used to calculate the difference in mechanical energy between these control points and then determine the outlet gas flow rate and well pressure.

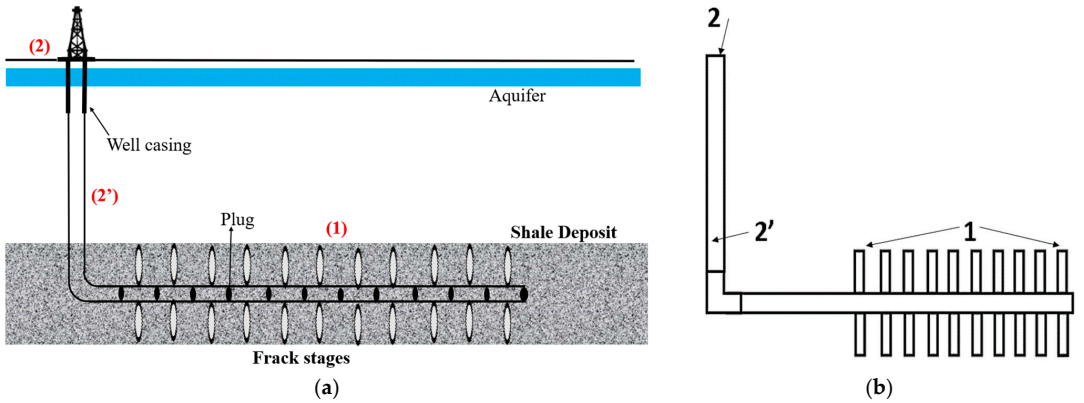

Figure 2. (**a**) Schematic representation of a shale gas well, indicating control points 1, 2′, and 2 for the application of Bernoulli's equation. (**b**) Simplified representation of gas flow ducts.

2.1.2. Governing Equations

The present model is based on the coupled solution of Bernoulli's equation and the gas mass conservation equation. When a pressure difference is applied to a well, a flow rate is established to drive out the contained fluid. An unconventional well has an additional feature: the gas is confined in three locations as explained above. This characteristic can be included in the flow rate calculations if the mass conservation equation includes a gas source term that releases gas according to the actual production curve, mimicking the production kinetics of adsorbed and dissolved gas.

The system can be simplified to a set of cracks connected to the main duct as shown in Figure 2b. The corresponding hydraulic resistance diagram is shown in Figure 3. Notice that crack resistances are connected in parallel, but all of them converge to the main duct resistance. Point 1 is a plurality of points, the tips of all cracks, and point 2 is the ground level. Gas flows from point 1 to point 2, i.e., each crack contributes to the total gas flow rate.

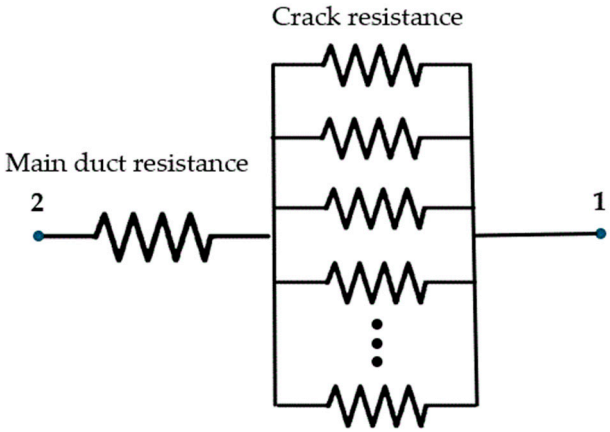

Figure 3. Hydraulic resistance diagram for an unconventional natural gas well.

Let us consider first Bernoulli's equation, which is a balance of the mechanical energy of fluid between points 1 and 2, for steady-state conditions [21].

$$\int_{p_1}^{p_2} \frac{dp}{\rho} + \frac{1}{2}\left(v_2^2 - v_1^2\right) + g(z_2 - z_1) + K\prime v_2^2 = 0, \quad (2)$$

where p_1 and p_2 are absolute pressures, MPa; g is the acceleration of gravity, 9.8 m/s^2; v_1 and v_2 are the mean gas velocities, m/s; ρ is the local gas density, kg/m^3; z_1 and z_2 are the heights from the bottom of the well; and K′ is a dimensionless coefficient for friction energy losses, and its value is specific for each fracked well. This coefficient can be properly determined using the first measurement points of the gas flow rate released from the well, that is, the initial free gas flow rate. In this early and short production step, quasi-steady-state conditions are assumed, and since the flow rate and pressure are known and only free gas flows out, this leaves coefficient K′ as the only unknown in Equation (2). In contrast, theoretical determination of K′ would require hard-to-obtain data since energy losses depend on the effective soil permeability, which is a function of the level of subsoil fracturing, that is, the number, dimensions, tortuosity, and interconnectivity of cracks, and other variables such as the particle size of the proppant, which also has an effect on the overall permeability and fluid flow rate [20].

Point 1 has the following data: $v_1 = 0$ because the gas is at rest in the bottom of the well, and gas acceleration occurs gradually; $z_1 = 0$. Point 2 is characterized by the following data: $v_2 = W/(\rho A_d)$, where W is the gas mass flow rate (kg/s) at the duct cross-sectional area, A_d, and z_2 = average well depth (m).

Determination of pressure energy change

When the gas rises to the surface, it will lose considerable pressure; therefore, it was considered that the gas is a compressible fluid. Gas density is a function of pressure. The choice of this function depends on what type of gas expansion phenomenon is considered. Adiabatic expansion represents most of the gas expansion phenomena, since there is no heat transfer between a gas and its surroundings. This expansion leads to a decrease in the gas temperature. However, this decrease should have a limit. Imagine the gas is cooling down while flowing through the duct. If it reached 0 °C (water freezing point), then liquid water from the fracking suspension would act as a thermal damper. It would provide heat to the gas, stabilizing its temperature. From this point, adiabatic expansion would switch to isothermal expansion at 0 °C. Let us call point 2′ the position where this switch occurs. The total pressure energy change of the gas can be calculated from the following expression.

$$\int_{p_1}^{p_2} \frac{dp}{\rho} = \int_{p_1}^{p_{2\prime}} \frac{dp}{\rho_{adiab}} + \int_{p_{2\prime}}^{p_2} \frac{dp}{\rho_{isotherm}} \tag{3}$$

For an adiabatic expansion, the density depends on pressure according to the following equation:

$$\frac{1}{\rho_{adiab}} = \sqrt[\gamma]{\frac{K}{p}}, \tag{4}$$

where γ is the ratio of specific heats at constant pressure and at constant volume of natural gas. This coefficient is equal to 1.28 for methane, and K is a constant that is evaluated using known conditions of gas pressure and temperature, for example, those corresponding to point 1.

Once the gas reaches a temperature of 0 °C, then isothermal expansion begins. The density can be written as a function of pressure assuming real gas behavior, according to the following equation:

$$\frac{1}{\rho_{isotherm}} = \frac{ZRT_{2\prime}}{M} \cdot \frac{1}{p}, \tag{5}$$

where Z is the compressibility factor, R is the universal gas constant, and $T_{2'}$ is the assumed absolute temperature of gas, that is, 273.15 K (0 °C). Therefore, Equation (3) can be integrated after substitution of Equations (4) and (5) into Equation (3).

Determination of coefficient of friction energy losses

The friction coefficient, K′, is a function of the characteristics of the gas transport media such as fractures, porous media, and the pipeline itself. This coefficient is proposed to be evaluated from Equation (2) using the first data points obtained during the earlier gas extraction step. The resulting expression is:

$$K\prime = \frac{\int_{p_2}^{p_1} \frac{dp}{\rho} - g\Delta z}{v_2^2} - \frac{1}{2} \tag{6}$$

Determination of gas pressure in the reservoir

Pressure p_1 depends on the concentration of free gas at the well. It starts at a value ${p_1}^0$ at t = 0 and decreases with time, $p_1(t)$. This decrement is proportional to the amount of free gas that has left the well. Assuming a real gas model, the instantaneous gas pressure in the well can be obtained from the gas flow rate leaving the well, as shown in Appendix A.1, and the resulting equation is:

$$p_1 = p_1^0 - \left(\frac{ZRT_1}{MV_{well}}\right) \cdot \int_0^t W dt, \tag{7}$$

where M is the molecular mass of the gas, kg/mol; Z is the gas compressibility factor; R is the universal gas constant, J/(mol · K); T_1 is the absolute temperature of the gas in the cracks, K; and W is the gas mass flow rate, kg/s. Finally, V_{well} is the space, m^3, that is

available for free gas. It includes cracks and interconnected pores and cannot be measured directly, but it can be determined assuming the following. Consider the period, tfree, where the gas flow rate vs. time curve is a straight line, i.e., it is a linear function. During this production step, only free gas is released. Therefore, V_{well} was determined as the amount of all free gas, which was readily obtained integrating the gas flow rate over period tfree. This volume is expressed by the following equation.

$$V_{well} = \int_0^{tfree} \frac{W}{\rho_1} dt \tag{8}$$

Equation (7) only applies to the linear period of gas production. To obtain the equation for pressure during the whole lifetime of the well, new free gas that sources from desorption and diffusion was considered as follows. First, during the initial period of gas production, there is no kerogen gasification. However, after the former free gas leaves the well, desorption from the pore surface and diffusion through the kerogen occurs, releasing free gas, which contributes to increasing the well pressure. From these physical characteristics of the process, the present authors postulate the following semi-empirical power-law expression for the pressure source term, Δp_{ST}.

$$\Delta p_{ST} = B\left(1 - \frac{p_1}{p_1^0}\right)^a + C\left(1 - \frac{p_1}{p_1^0}\right)^b, \tag{9}$$

where a, b, B, and C are specific constants for every fracked well, and the ratio $p_1/{p_1}^0$ is a dimensionless pressure, which is always less than or equal to one. The amount $1 - p_1/{p_1}^0$ is the free gas relative pressure decrease during production. This quantity is very close to zero when p_1 is close to ${p_1}^0$; then, p_{ST} approaches to zero, as expected for the earlier step of free gas recovery. However, when p_1 decreases, it triggers the mechanisms of desorption and diffusion of methane, and accordingly, p_{ST} becomes important. Adding the pressure source, Δp_{ST}, to Equation (7) results in:

$$p_1 = p_1^0 - \left(\frac{ZRT_1}{MV_{well}}\right) \cdot \int_0^t W dt + \Delta p_{ST} \tag{10}$$

This equation expresses the pressure evolution in the well as the combined result of extracting free gas and gasifying kerogen. Appendix A.2 shows an analogy between the air emptying from two interconnected compressors and the natural gas extracted from unconventional reservoirs. This analogy is aimed to provide a better qualitative understanding of Equation (10). Furthermore, the last section of Appendix A.3 includes a qualitative physical chemistry analysis to justify this equation.

2.1.3. Solution Method

The unknown variables are the gas velocity, v_2, and the well pressure, p_1. The former is used to calculate the gas production flow rate, Q, and the second variable monitors the concentration of free gas in the well. Two unknowns require two independent equations. Equation (2) was solved simultaneously with Equation (10). Since Equation (2) applies for steady-state conditions, the gas production curves were represented by a series of stepwise steady states, each under a constant gas flow rate, similarly to the pressure–time curves. These stepwise periods were connected by instantaneous drops in pressure or the gas flow rate. Figure 4 shows stepwise steady states representing a typical gas flow rate curve. The time scale was divided into a number of temporal nodes, t_1, t_2, t_3,. . ., t_n, mutually separated by a time step value, Δt. Our study cases were solved using a variable time step.

The model parameters include the friction coefficient, K', and the pressure source term constants, a, b, B, and C, all of which are unknowns. These parameters were determined numerically by minimizing the difference between the computed and measured gas flow

rate and pressure. This was achieved by trial and error using an excel worksheet, although an automated method such as a multidimensional gradient method may be appropriate. Figure 5a,b shows the flow charts for the algorithm used. Figure 5a describes the calculation of coefficient K′. An initial estimate of K′ was calculated from Equation (6) using the values of v_2 determined from the smoothed flow rate curve at time nodes t_1, t_2, etc. Pressure p_1 was calculated from Equation (7) at the same time nodes. Equations (7) and (8) were computed numerically using the trapezoid method. Only a few initial gas flow rate data were used for these calculations, since at the earlier extraction stage, there is no gasification of kerogen that may interfere with estimation of K′.

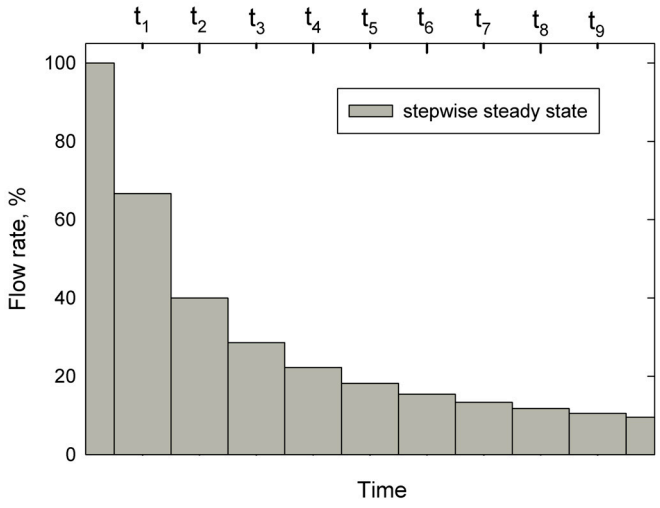

Figure 4. Representation of a gas flow rate curve using stepwise steady states.

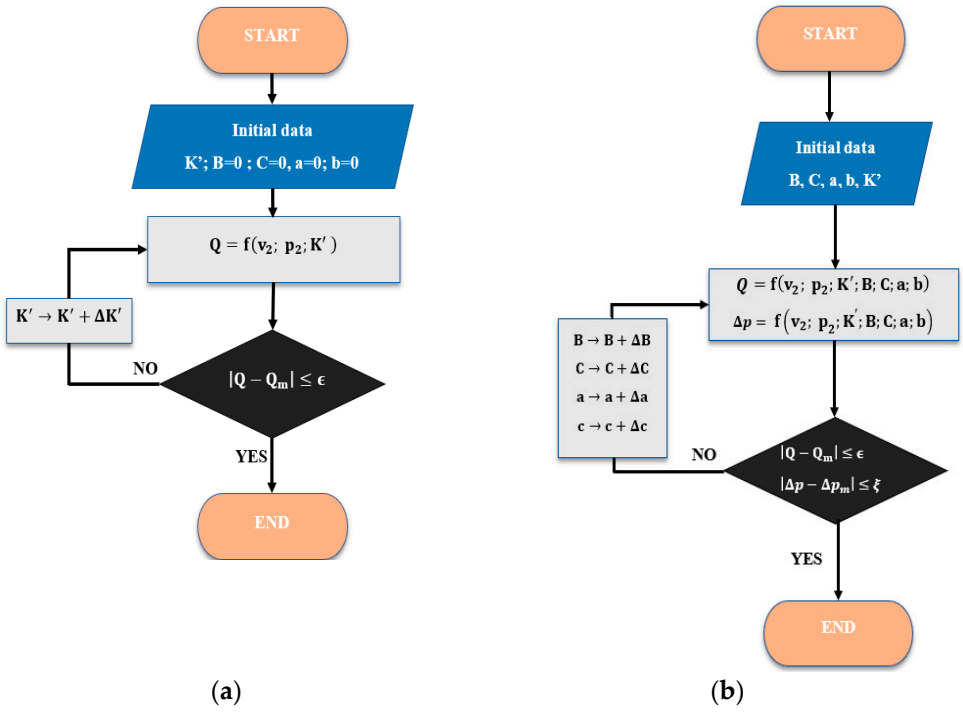

(**a**) (**b**)

Figure 5. Algorithms for calculating the gas production parameters in the well: (**a**) the flow diagram for the calculation of the friction coefficient (K′), (**b**) the flow diagram for the determination of the coefficients of the pressure source term model (B, C, a, and b).

The computed K′ values at each time node were averaged, and using this average value, the gas velocity v_2 was computed using Equation (2) for the same nodes, t_1, t_2, etc.

The gas flow rate, Q, was estimated from this velocity and compared with the corresponding smoothed measurements, Q_m. If the absolute difference $|Q - Q_m,| < \varepsilon$, then the obtained K′ was satisfactory; otherwise, K′ was modified by a trial amount ΔK′ and velocity v_2 was calculated again. The limit error ε was chosen as $\varepsilon = 0.02\ Q_m$. Notice that mutual agreement of the gas flow rates was aimed for only the first data points, not for the whole flow rate curve. Figure 5b shows the calculation process for coefficients a, b, B, and C. In contrast with the previous calculations, this case used all data points. Initial guess values were assumed for the coefficients, and velocity v_2 was calculated with Equation (2) and well pressure p_1 using Equation (10). Similarly to the previous calculations, if the calculated quantities disagreed with the respective measurements, then the constants were modified, and the calculation process was repeated iteratively until reaching ε and ξ tolerances.

Note that the coefficients of the power-law model (B, C, a, and b) are constants that modulate the magnitude of the pressure source term, Δp_{ST}, such that the computed flow rate and pressure curves agree with the corresponding measurements for the whole studied period of gas extraction.

3. Results and Discussion

3.1. Calculation of Friction Factor, K′

Figure 6a,b shows the comparison between the data smoothed and calculated curves of the gas production rate as a function of time in wells "A" and "B", respectively. The blue curve represents the rate of gas production calculated by Bernoulli's equation when pressure was calculated with Equation (7). The value of K′ was determined to match the computed gas flow rate with the corresponding initial flow points of the actual gas production data. Figure 6a,b shows an excellent agreement between the computed and smoothed curves in the initial period of time. Additionally, it can be noted that the calculated curve decays sharply in a short time. This is the expected behavior if there were only free gas in the reservoir, i.e., no methane, no kerogen. It should be noted that the friction factor is a magnitude that characterizes the fluid flow resistance of a fracked well. Therefore, this factor is also valid for the whole gas extraction period.

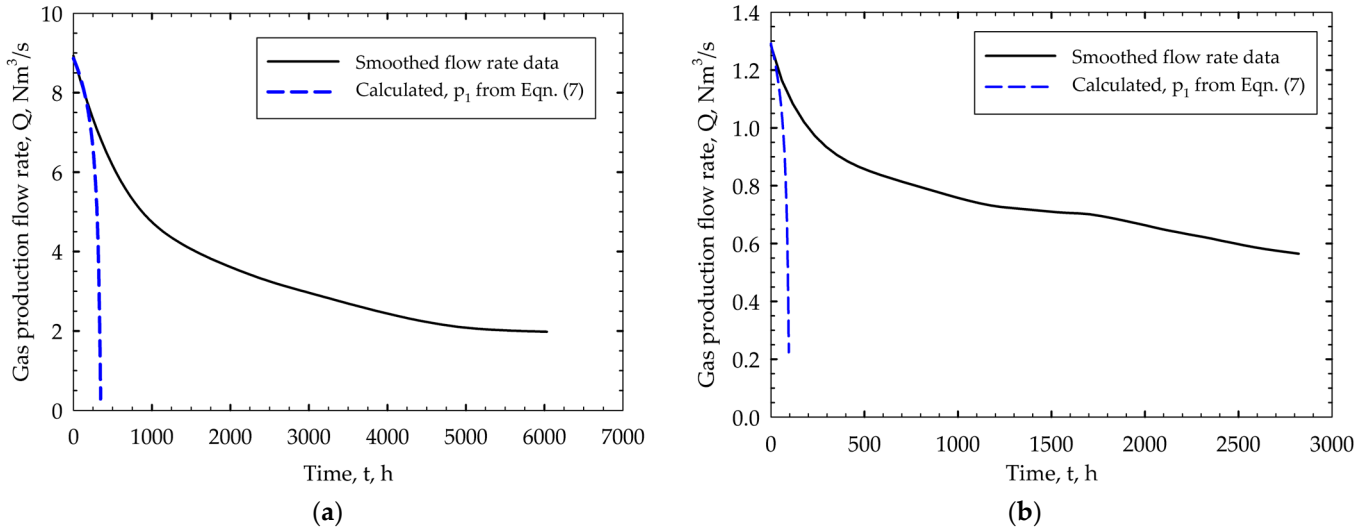

Figure 6. Comparison of smoothed data and calculated production curves using pressure p_1 that was computed from Equation (7). (**a**) Well "A" and (**b**) well "B".

3.2. Calculation of Coefficients from the Pressure Source Term

Figure 7a,b shows the comparison between the measured and calculated curves of the gas production rate as a function of time in wells "A" and "B", respectively. The red curve represents the gas production rate calculated by Bernoulli's equation considering the pressure generated by the gas released from desorption and diffusion. This is the final

curve obtained after optimizing coefficients a, b, B, and C of the pressure source term, Δp_{ST}. There is an excellent agreement between both curves. The Pearson correlation coefficients were 0.97 and 0.96 for wells "A" and "B", respectively. The pressure source term accounts for the gradual release of methane adsorbed and dissolved in the kerogen, which depends on the instantaneous pressure of free gas remaining in the reservoir.

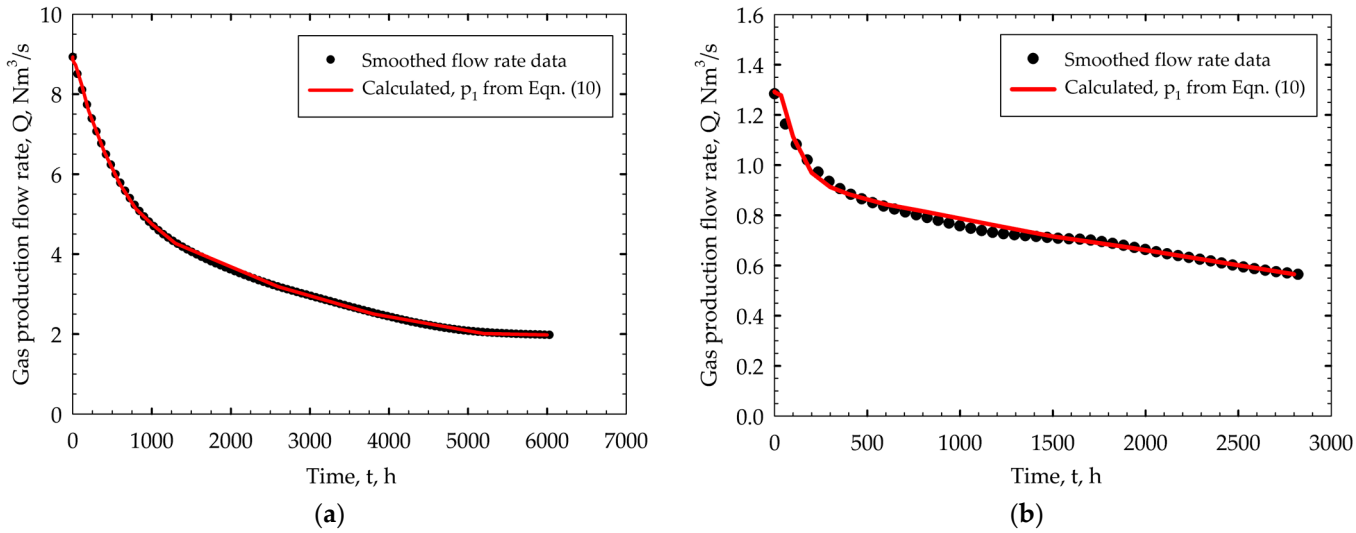

Figure 7. Comparison of smoothed data and calculated gas flow rate curves using pressure p_1 that was computed from Equation (10). (**a**) Well "A" and (**b**) well "B".

In order to visualize the extrapolation values of the gas flow rate at long times, the data from Figure 7a,b have been replotted in log–log scales in Figure 8a,b. Furthermore, Figure 8c,d shows the log–log plots for the computed and smoothed data pressure drop ($p_1 - p_2$) curves for wells "A" and "B", respectively. The computed pressure drop curves remarkably agree with the corresponding smoothed curves. Pearson correlation coefficients of 0.98 and 0.97 were computed for measurements of wells "A" and "B", respectively. Moreover, the computed curves can be used to extrapolate in time both magnitudes, anticipating the total life period of these wells.

Table 2 summarizes the obtained values of the five coefficients for both wells. The friction factor, K', for well "A" is considerably smaller than the corresponding value for well "B". This suggests that the overall crack and porous network cross-sectional area that carries the gas from well "A" is much larger than for well "B". The respective applied pressures and the consequent initial gas flow rates led to this conclusion. Regarding exponents a and b that appear in Equation (10), it is noticeable that they have the same values for both wells. This is a coincidence since no physical meaning is attributed to these dimensionless exponents. Finally, coefficients B and C have the same magnitude but opposite sign. Similarly to the exponents, this may be coincidental, although they should have opposite signs to calculate a maximum value for the pressure source and then a decrease for this variable. Coefficients B and C have pressure units and may be related to the characteristics of the reservoir, such as the total carbon, nanopore size distribution, rock permeability, etc. Theoretical prediction of these coefficients suggests a potential line for future research.

Table 2. Model coefficients determined from natural gas production curves.

Coefficients	K'	a	b	B (MPa)	C (MPa)
Well "A"	8.61	5	3	−62.2	62.2
Well "B"	408	5	3	−7.0	7.0

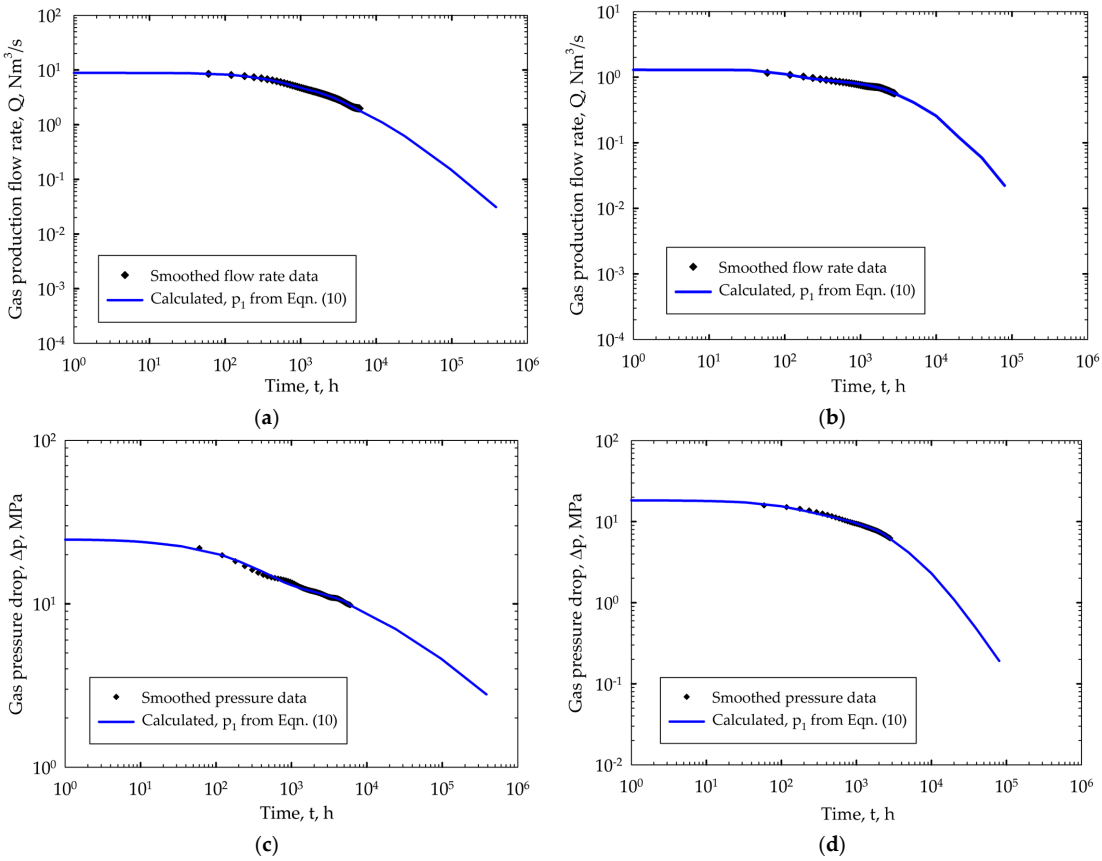

Figure 8. Log–log plots comparing the smoothed data and computed curves of the gas flow rate for (**a**) well "A" and (**b**) well "B", and of the gas pressure drop for (**c**) well "A" and (**d**) well "B". Computed results were obtained using Equation (10) for gas pressure. Calculated curves are extrapolated to long times, anticipating the lifetime of each well.

3.3. Sensitivity Analysis

Sensitivity analysis of model coefficients is helpful to understand the uncertainty and stability of model predictions. Two sensitivity analyses are presented. First, the sensitivity of the pressure source term with respect to each of its four parameters is presented. Then, the sensitivity of the gas flow rate with respect to three important parameters, the pipe diameter, well depth, and well temperature, is presented. Table 3 shows the computed sensitivity analysis of the pressure source term with respect to each coefficient, using the following derivatives.

$$\frac{\partial \Delta p_{ST}}{\partial B} = X_1^a \tag{11}$$

$$\frac{\partial \Delta p_{ST}}{\partial C} = X_1^b \tag{12}$$

$$\frac{\partial \Delta p_{ST}}{\partial a} = BX_1^a \ln X_1 \tag{13}$$

$$\frac{\partial \Delta p_{ST}}{\partial b} = CX_1^b \ln X_1 \tag{14}$$

where the free gas relative pressure decrease is defined as,

$$X_1 = \frac{p_1^0 - p_1}{p_1^0} \tag{15}$$

The values in the table were computed using the coefficients for well "A". The derivatives with respect to B and C have the same values for well "B" since coefficients a

and b are also equal to 5 and 3, respectively. The derivatives with respect to coefficients a and b for well "B" are proportionally smaller than the corresponding coefficients for well "A". The table shows that the derivatives have small absolute values when $X_1 \leq 0.2$ but have reasonable larger values when $X_1 > 0.2$. In this later case, pressure p_1 has decreased importantly, and kerogen may start to release free gas. Therefore, the sensitivity of the pressure source term becomes particularly important under this pressure. These results show favorable numerical conditions to reduce uncertainty and achieve stability during the solution process.

The second sensitivity analysis is on the computed gas flow rate. Figure 9a,c shows the computed gas flow rate for well "A" including the cases with ±10% variation in the pipe diameter, d(m), well depth, Δz(m), and well temperature, T(°C), respectively. For each figure, all of the rest of the variables are kept constant with the same values as the original case. All curves were calculated using the same model coefficients given in Table 2. The figures show a reasonable variation in the gas flow rate in response to each parameter, thus confirming the appropriate numerical conditions to reduce uncertainty and achieve numerical stability.

Table 3. Sensitivity analysis of the pressure source term. Data are for well "A".

X_1	$\frac{\partial \Delta p_{ST}}{\partial B}$	$\frac{\partial \Delta p_{ST}}{\partial C}$	$\frac{\partial \Delta p_{ST}}{\partial a}$	$\frac{\partial \Delta p_{ST}}{\partial b}$
0.01	0.000	0.000	0.000	0.000
0.2	0.000	0.008	−0.032	0.801
0.4	0.010	0.064	−0.584	3.648
0.5	0.031	0.125	−1.347	5.389
0.6	0.078	0.216	−2.471	6.863
0.8	0.328	0.512	−4.548	7.106
0.99	0.951	0.970	−0.594	0.607

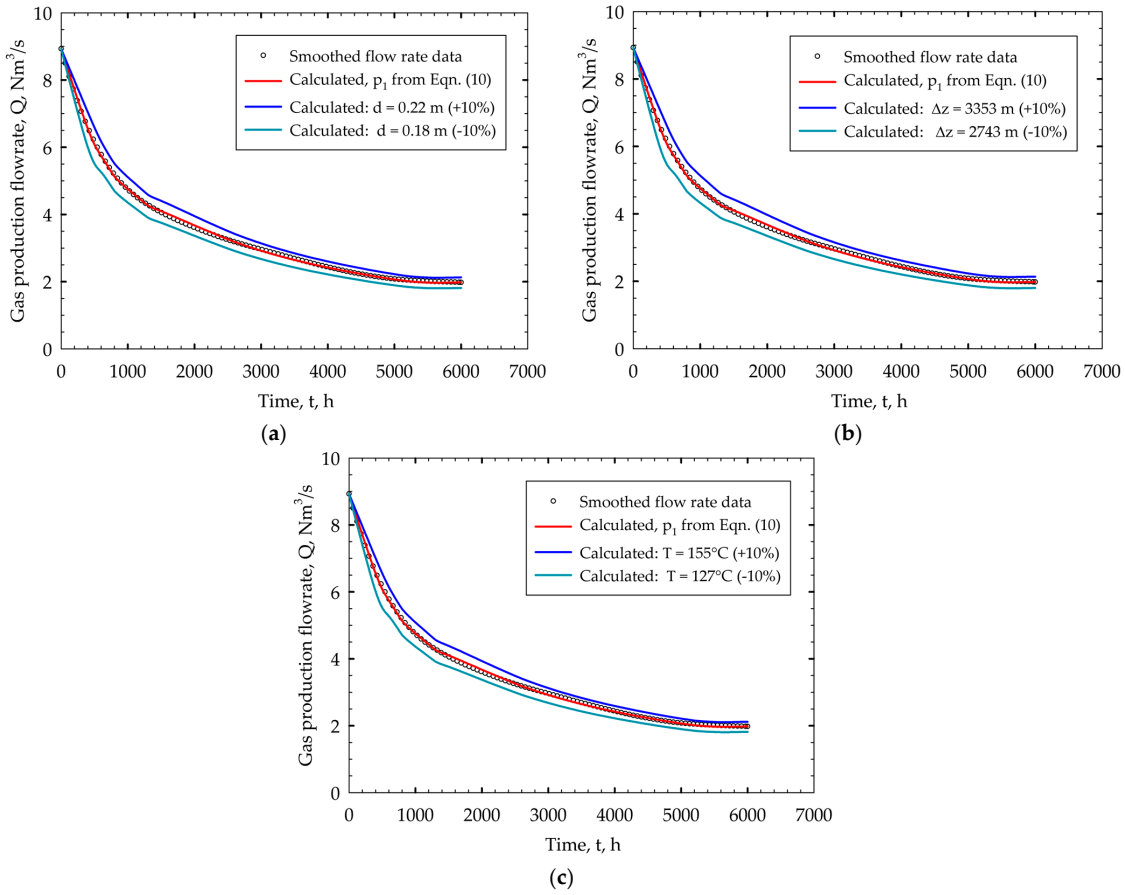

Figure 9. Computed sensitivity analysis of gas flow rate to three main parameters: (**a**) pipe diameter, (**b**) well depth, and (**c**) well temperature.

3.4. Comparative Analysis

In a recent paper, Coutry et al. [22] presented results on an assessment of the accuracy of empirical decline curve techniques to predict gas production in unconventional reservoirs. They studied fourteen decline curve methods, including the traditional Arps' method, which is given by the following empirical equation for the instantaneous gas flow rate, Q.

$$Q = \frac{q_0}{(1 + \beta D_0 t)^{1/\beta}}, \tag{16}$$

where q_0 is the initial gas flow rate, β is the Arps' decline curve exponent, and D_0 is the initial decline rate.

They tested the methods using production data from three wells in the United States and concluded that each method may be useful in different cases. A specific method should be chosen according to the characteristics and circumstances of each well. No universal method can be recommended for any well. Figure 10a,b shows the comparisons between the Arps' decline curves, the smoothed data curves, and the pressure source model (PSM) curves. Figure 10a corresponds to well "A" data. The PSM can follow accurately the smoothed curve, while the Arps' model fails at longer times. The Pearson correlation coefficient for the PSM was 0.97, while for the Arps' method, it was calculated as 0.89. Figure 10b shows the corresponding results for well "B". In this case, three curves calculated with the Arps' method are shown. None of them represent the smoothed data curve as closely as the calculated curve using the PSM. The Arps' curve, which is closer to the smoothed data curve, has a Pearson correlation coefficient of 0.5, which is much lower than the 0.96 value obtained with the PSM.

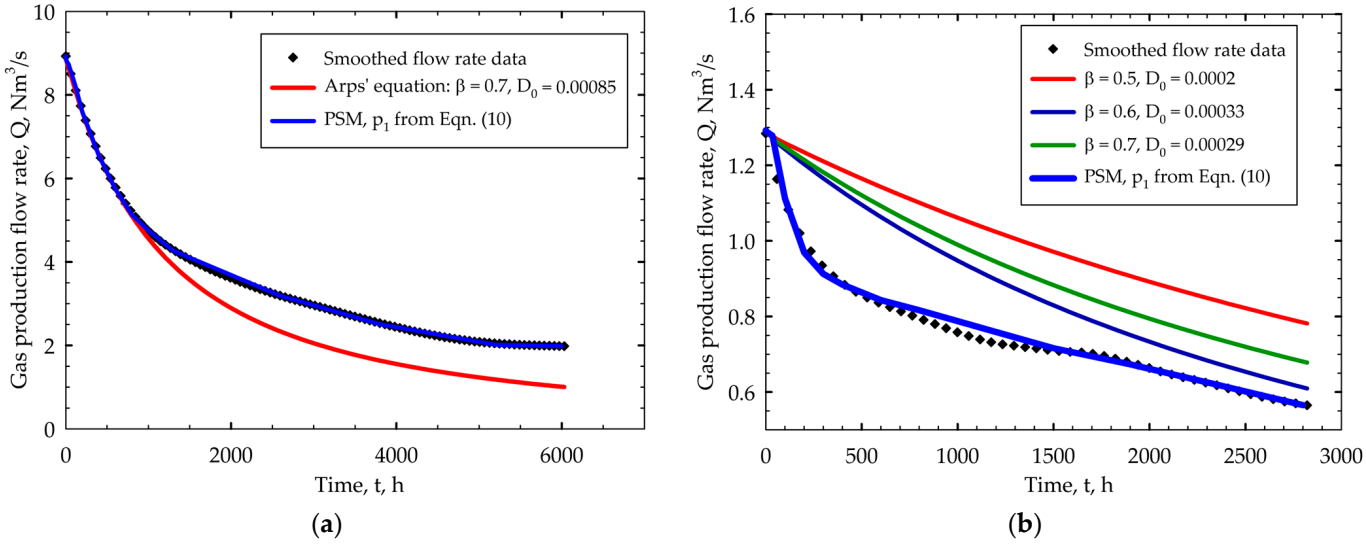

Figure 10. Comparison of Arps' decline curves with smoothed data curves and PSM curves for (**a**) well "A" and (**b**) well "B".

Additionally, Figure 11 shows a comparison between the PSM gas flow rate curve for well "A" and the corresponding computed curves using other models [23]. The models are the stretched exponential decline model (SEDM), the power law exponential (PLE) model, the Duong model, and of course the Arps' model. All model parameters were determined by regression analysis using the same smoothed data, which are also included in the figure.

These results show that the PSM, based on the transient solution of Bernoulli's equation and a semi-empirical pressure source equation, can improve the reliability of predictions over traditional empirical decline methods since it represents more accurately the actual measured data. A reason for this may be that the PSM considers both the gas flow rate and gas pressure, while the available decay models are only focused on the gas flow rate.

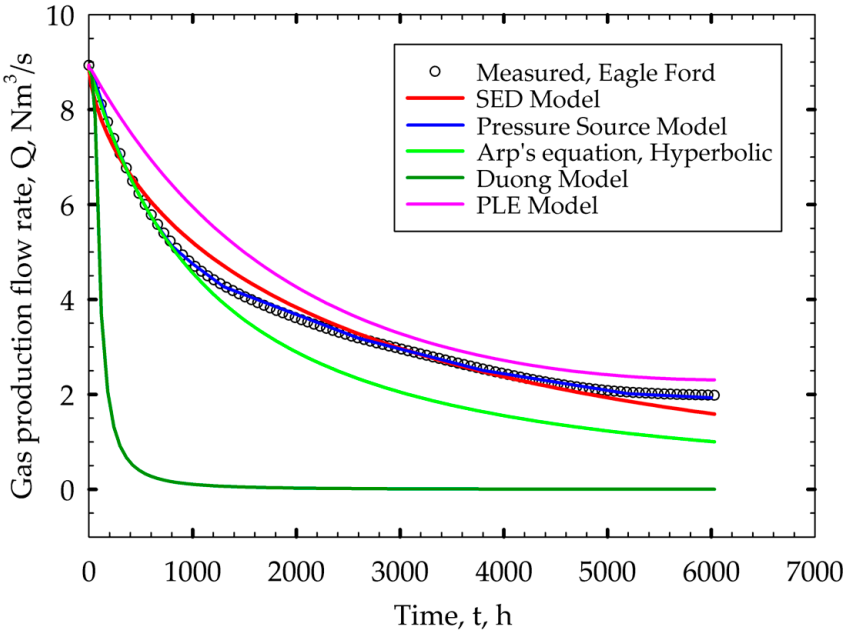

Figure 11. Comparison between the computed gas flow rate curves obtained with different models, including our pressure source model. The smoothed measurement data are remarkably better represented by the PSM.

3.5. Discussion of the Pressure Source Term

Gas release occurs through diffusion and desorption processes of the methane in the kerogen. These processes are activated after the free gas, located in interconnected cracks and pores, begins to be removed. The following equilibrium equation clarifies this process.

$$CH_{4(g)} \Leftrightarrow [CH_4]_{kerogen} \quad (17)$$

This equation expresses a thermodynamic equilibrium between free methane in the form of gas and methane dissolved in organic matter. When free gas is removed, its pressure decreases. This allows the reaction to be shifted to the left side according to its equilibrium constant or according to Le Chatelier's principle. However, the above equilibrium occurs only at the interface between the organic matter and the cracks. A diffusive process of methane from the bulk of the organic matter is required to supply the methane removed at the interface.

Figure 12a,b shows plots of the computed pressure source term, Δp_{ST}, as a function of the pressure drop, $p_1 - p_2$, and as a function of the free gas relative pressure decrease, X_1, as defined by Equation (15), respectively. Figure 12a shows the computed pressure source for both wells, indicating that at their initial pressure drop values, 25 and 18.5 MPa, both pressure sources are equal to zero. However, when the pressure drop decreases, the pressure source increases gradually, mimicking the gradual gasification of kerogen. The pressure source reaches a maximum value in both wells and then finally declines to zero. Figure 12b represents the same data but plotted in terms of X_1. In this case, both curves have been normalized in the horizontal axis; therefore, both share the same initial point, $X_1 = 0$.

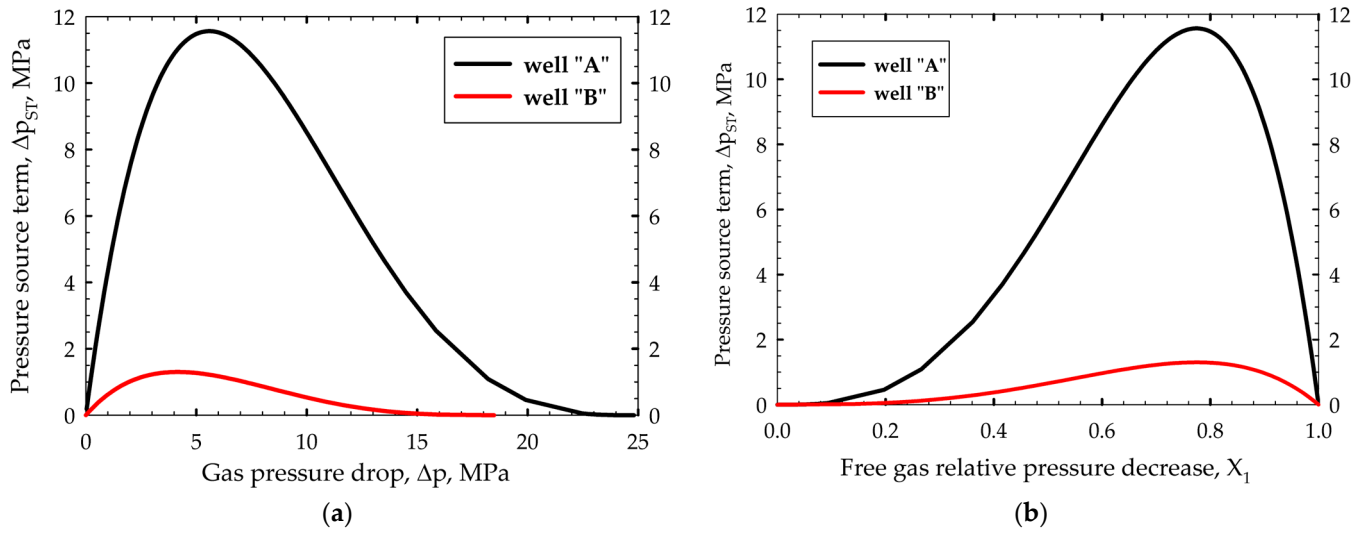

Figure 12. Computed pressure source term for both wells, as a function of: (**a**) pressure drop, p_1-p_2, and (**b**) free gas relative pressure decrease, X_1, defined by Equation (15).

3.6. Production Data Analyzed under Darcy's Law and Ergun Equation

Darcy's law, Equation (1), is an expression for the gas pressure drop as a linear function of the gas flow rate. As discussed in the Introduction section, the permeability, defined in that equation, has been determined by many authors as a function of other variables to represent actual laboratory or field data. This is evidence that the pressure and gas flow rate are not related by a linear function. On the other hand, the Ergun equation, which is readily found in the porous media literature, shows a parabolic relationship between these variables, written as follows:

$$\frac{\Delta p}{L} = \alpha_1 Q + \alpha_2 Q^2 \tag{18}$$

where L is the distance between the points where the pressure drop Δp is measured, Q is the flow rate through the porous medium, and α_1 y α_2 are coefficients that depend on the characteristics of the porous medium such as the pore size, tortuosity, porosity, and the density and viscosity of the fluid. Indeed, this equation is reduced to Darcy's law when $\alpha_2 = 0$. Therefore, the Ergun equation is a more general expression that includes two contributions to the pressure drop: a laminar flow contribution, given by the linear term, $\alpha_1 Q$, and a turbulent flow contribution, represented by the quadratic term, $\alpha_2 Q^2$. Can this equation represent actual natural gas production data?

Figure 13 shows gas flow rate versus pressure drop plots of the smoothed data and the PSM curves for both wells. As with previous results, there is an excellent agreement between them. Moreover, the curve for well "A" resembles a parabolic function, while the curve for well "B" is nearly a straight line. This means that the Ergun equation can be used to represent the pressure drop as a function of the gas flow rate. Nevertheless, the best correlation function for these cases corresponds to the PSM.

A final comment is worthwhile to mention. Differently from the empirical models that are available to predict production decay, the PSM is based on the principles of conservation of mechanical energy and gas mass and includes a semi-empirical pressure source term to represent kerogen gasification during production. This model has shown the importance of considering pressure evolution for a more comprehensive fluid flow characterization leading to accurate gas flow rate predictions.

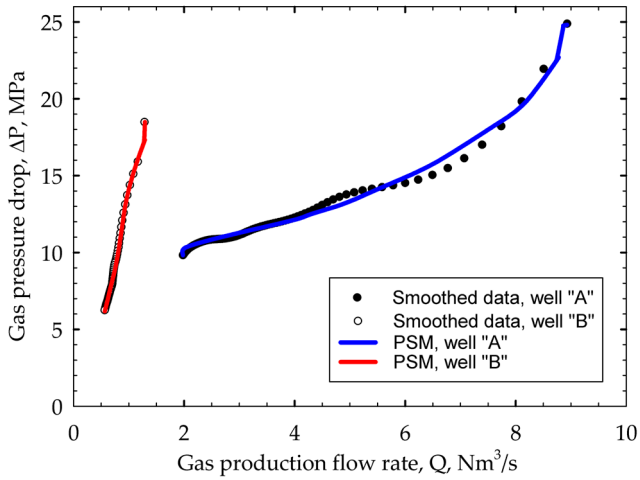

Figure 13. Plots of gas flow rate versus gas pressure drop comparing smoothed data and PSM curves for both wells.

4. Summary and Conclusions

This work presents and validates a new mathematical model to calculate the evolution of gas pressure and flow rate during the production period of unconventional reservoirs. This model is based on the principle of conservation of mechanical energy, expressed by Bernoulli's equation. The transient nature of the gas extraction process is approached by steady-state stepwise periods. The pressure is computed from the free gas amount available in the cracks, pores, and main duct in the well. A pressure source term accounts for the kinetics of desorption and diffusion of methane. The five model parameters were obtained from gas production data of wells in the Eagle Ford [K′ = 8.61, B = −62.2, C = 62.2, a = 5, and b = 3] and Burgos basins [K′ = 408, B = −7.0, C = 7.0, a = 5, and b = 3].

The predicted evolution of gas pressure and flow rate fully agree with the corresponding smoothed data points curves, finding Pearson correlation coefficients above 0.95 for flow rate and pressure drop data and for both studied wells. This means that constant model coefficients allow for the calculation of the evolution of both the gas pressure and flow rate for each well.

A comparison of the curves obtained from regression on smoothed production data using the PSM, Arps' model, PLE model, SED model, and Duong model showed a remarkable improvement when using the PSM. A reason for this may be that, differently from the available decay models, the pressure source model considers both the gas flow rate and gas pressure evolution and is based on mechanical energy and mass conservation principles. The decay models only consider gas flow rate data.

The postulated power-law function representing the pressure source term was able to mimic the desorption and diffusion phenomena. These processes provided free gas to the cracks and macropores after decay of the initial gas pressure.

The measured gas pressure–flow rate curves follow a parabolic function in agreement with the Ergun equation for porous media. The present model results also agree with this parabolic function.

Author Contributions: Conceptualization, B.Y. is the main author of this paper since the present work is part of his PhD thesis developed under the supervision of F.A.A.-G.; methodology, B.Y.; software, B.Y.; validation, B.Y.; formal analysis, B.Y. and F.A.A.-G.; investigation, B.Y.; resources, F.A.A.-G.; data curation, B.Y.; writing—original draft preparation, B.Y.; writing—review and editing, F.A.A.-G.; visualization, B.Y.; supervision, F.A.A.-G.; project administration, F.A.A.-G.; funding acquisition, F.A.A.-G. All authors have read and agreed to the published version of the manuscript.

Funding: This research was funded by CONACYT-SENER-HIDROCARBUROS [grant # 267962].

Data Availability Statement: An additional excel file has been submitted. It includes data points and important results. Original contributions generated in this study are included in the article; further inquiries can be directed to the corresponding author.

Acknowledgments: We thank CONACYT for the scholarship granted to B.Y. to carry out his PhD thesis. The authors thank the Library of the National Lithotheque of Mexico for the gas production data in the Mexican territory.

Conflicts of Interest: The authors declare no conflicts of interest. The funders had no role in the design of the study; in the collection, analyses, or interpretation of data; in the writing of the manuscript; or in the decision to publish the results.

Appendix A. Pressure Source Term

The pressure source model introduces a pressure source term, Δp_{ST}, in the well pressure, p_1, which is given by:

$$\Delta p_{ST} = B\left(1 - \frac{p_1}{p_1^0}\right)^a + C\left(1 - \frac{p_1}{p_1^0}\right)^b \tag{A1}$$

This is a semi-empirical equation proposed for the first time in the present work, and it aims to represent the gasification kinetics of kerogen during natural gas extraction. Because of its semi-empirical nature, no formal derivation for this equation is offered. However, to share the authors' thoughts behind this equation, three helpful concepts are presented in this appendix. The first one is the derivation of Equation (7), which is a relationship between the pressure in the well and the free gas mass flow rate. The second one is aimed to explain qualitatively Equation (10) by using an analogy between the air flowing out from two compressors hypothetically connected via a safety valve and the natural gas flowing from an unconventional reservoir. Finally, the third one is a physical chemistry qualitative analysis to justify the postulation of the pressure source term.

Appendix A.1. Gas Pressure and Gas Flow Rate

The gas pressure, p, in a closed well of volume capacity V_{well} is expressed by the real gas model as:

$$pV_{well} = ZnRT, \tag{A2}$$

where Z is the compressibility factor, R is the gas constant (8.31 J/mol K), T is the absolute temperature (K), and n is the number of gas mols, which is given by,

$$n = \frac{m}{M}, \tag{A3}$$

where m is the free gas mass in the closed well and M is its molecular mass. Substitution of Equation (A3) into Equation (A2) leads to the following expression.

$$pV_{well} = \frac{ZmRT}{M} \tag{A4}$$

Now, consider that the well is opened and a differential gas mass, dm, flows out the well. If all variables remain constant except the pressure, the corresponding pressure variation, dp, is obtained by differentiation of Equation (A4) obtaining the following equation.

$$dp = \frac{ZRT}{MV_{well}}dm \tag{A5}$$

Integrating the previous equation from pressure p_1^0 to p_1 and from mass 0 to m results in the following expression.

$$p_1 = p_1^0 + \int_0^m \frac{ZRT}{MV_{well}} dm \quad (A6)$$

The gas mass flow rate, W(kg/s), is used to determine dm, as dm = −W dt. Then, Equation (A6) becomes Equation (A7), given in the main text.

$$p_1 = p_1^0 - \int_0^t \frac{ZRT}{MV_{well}} W dt \quad (A7)$$

Appendix A.2. Analogy of Air Flow from Two Connected Compressors

Figure A1 shows two interconnected compressors. Let us turn on both closed compressors until reaching pressures p_I and p_{II}. Then, shut off both and disconnect the power. Now, let us empty both compressors. Air in compressor I can flow out to the atmosphere and represents the free natural gas in a reservoir. Compressor II is hypothetically connected to compressor I through a safety valve. Thus, no air leaves to the atmosphere through this safety valve. The valve will remain closed as long as the pressure difference between the compressors is smaller than a specified value, that is,

$$p_{II} - p_I < Set - pointpressure \quad (A8)$$

Air in compressor II represents the dissolved and adsorbed methane in kerogen. This air cannot leave directly to the atmosphere but first should flow to compressor I. The safety valve emulates the physical barrier to gasify kerogen: the pressure of free gas in the well. That is, the pressure in compressor I should decrease enough so that air from compressor II can push out the safety valve door and flow to compressor I.

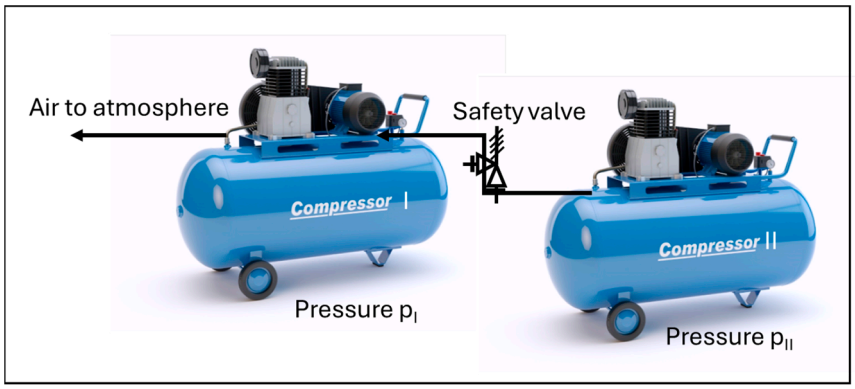

Figure A1. Schematic representation of interconnected compressors through a safety valve to explain its analogy with unconventional natural gas reservoirs.

Qualitatively, Equation (10) represents the pressure in compressor I. This pressure evolves because of an air flow output to atmosphere, which would be represented by the term

$$\left(\frac{ZRT_1}{MV_{well}}\right) \cdot \int_0^t W dt,$$

and an air flow input from compressor II, which would be represented by the term

$$\Delta p_{ST}$$

Appendix A.3. Theoretical Support for the Pressure Source Term

The pressure source term, defined by Equation (9), can also be visualized as follows. When the well is closed, free methane is in natural cracks and porous rock. This gas is in thermodynamic equilibrium with the methane that is dissolved in kerogen. This equilibrium is a dynamic process in which the rate of methane vaporization from kerogen is equal to the rate of methane condensation on the kerogen. Assuming constant temperature, the rate of vaporization is a function of the methane content in the kerogen, while the rate of condensation of methane is a function of the gas methane pressure.

Figure A2 shows a schematic plot of the rates of methane vaporization and condensation as a function of time. When the well is closed, these rates are mutually equal since they are in equilibrium. However, when the well is opened, the free gas leaves out from the well and its pressure decreases. Then, the condensation rate decreases, and the rate of vaporization dominates the net methane flow rate. Nevertheless, the rate of vaporization will also decrease since it depends on the methane content in the kerogen. The pressure source term is associated with the moles of gas that are released from the kerogen due to the difference between the evaporation and condensation rates. Notice that this difference is initially very small, then increases to reach a maximum value, and finally decreases to zero. Equation (9) is a postulated semi-empirical equation that follows such a behavior.

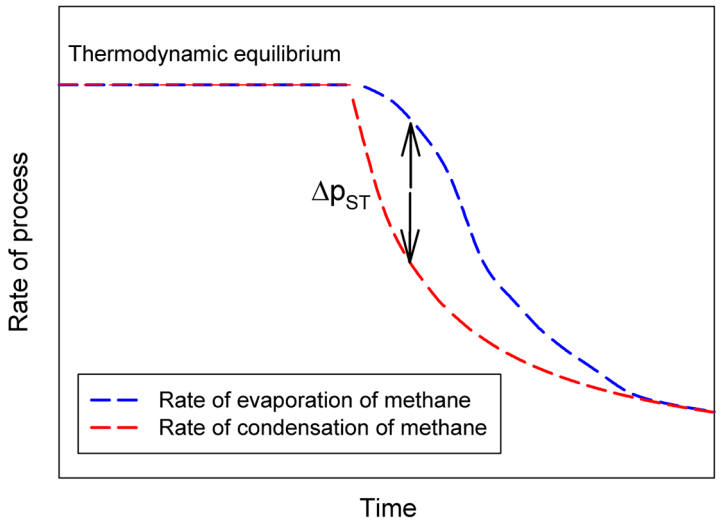

Figure A2. Schematic representation of the evolution of the rates of evaporation and condensation of methane during natural gas production. The pressure source term depends on the difference between these rates.

References

1. Etminan, S.R.; Javadpour, F.; Maini, B.B.; Chen, Z. Measurement of Gas Storage Processes in Shale and of the Molecular Diffusion Coefficient in Kerogen. *Int. J. Coal Geol.* **2014**, *123*, 10–19. [CrossRef]
2. Chalmers, G.R.; Bustin, R.M.; Power, I.M. Characterization of Gas Shale Pore Systems by Porosimetry, Pycnometry, Surface Area, and Field Emission Scanning Electron Microscopy/Transmission Electron Microscopy Image Analyses: Examples from the Barnett, Woodford, Haynesville, Marcellus, and Doig Units. *AAPG Bull.* **2012**, *96*, 1099–1119. [CrossRef]
3. Curtis, J. Fractured Shale-Gas Systems. *AAPG Bull.* **2002**, *86*, 1921–1938. [CrossRef]
4. Fathi, E.; Akkutlu, I. Matrix Heterogeneity Effects on Gas Transport and Adsorption in Coalbed and Shale Gas Reservoirs. *Transp. Porous Media* **2009**, *80*, 281–304. [CrossRef]
5. Nobakht, M.; Mattar, L.; Moghadam, S.; Anderson, D. Simplified Forecasting of Tight/Shale-Gas Production in Linear Flow. *J. Can. Pet. Technol.* **2012**, *51*, 476–486. [CrossRef]
6. Javadpour, F.; Singh, H.; Rabbani, A.; Babaei, M.; Enayati, S. Gas Flow Models of Shale: A Review. *Energy Fuels* **2021**, *35*, 2999–3010. [CrossRef]
7. Arevalo, J.A.; Castellanos, F.; Pumar-Martínez, F. Dynamic Characterization of Unconventional Gas Reservoirs: Field Cases. In Proceedings of the 2nd Unconventional Resources Technology Conference, Denver, CO, USA, 25–27 August 2014; American Association of Petroleum Geologists: Denver, Colorado, USA, 2014. [CrossRef]

8. Song, W.; Yao, J.; Li, Y.; Sun, H.; Yang, Y. Fractal Models for Gas Slippage Factor in Porous Media Considering Second-Order Slip and Surface Adsorption. *Int. J. Heat Mass Transf.* **2018**, *118*, 948–960. [CrossRef]
9. Li, Z.; Qi, Z.; Yan, W.; Xiang, Z.; Ao, X.; Huang, X.; Mo, F. Prediction of Production Performance of Refractured Shale Gas Well Considering Coupled Multiscale Gas Flow and Geomechanics. *Geofluids* **2020**, *2020*, 9160346. [CrossRef]
10. Younk, N. The Impact of Hyperbolic Decline Curve Parameters on Long-Term Production Forecast Accuracy for Unconventional Oil and Gas Production. Master's Thesis, Montana Technological University, Butte, MT, USA, 2020; pp. 105–110.
11. Wang, J.; Bentley, Y. Modelling World Natural Gas Production. *Energy Rep.* **2020**, *6*, 1363–1372. [CrossRef]
12. Sang, Q.; Li, Y.; Yang, Z.; Zhu, C.; Yao, J.; Dong, M. Experimental Investigation of Gas Production Processes in Shale. *Int. J. Coal Geol.* **2016**, *159*, 30–47. [CrossRef]
13. Singh, H.; Cai, J. Permeability of Fractured Shale and Two-Phase Relative Permeability in Fractures. In *Petrophysical Characterization and Fluids Transport in Unconventional Reservoirs*; Elsevier: Amsterdam, The Netherlands, 2019; pp. 105–132. [CrossRef]
14. Darabi, H.; Ettehad, A.; Javadpour, F.; Sepehrnoori, K. Gas Flow in Ultra-Tight Shale Strata. *J. Fluid Mech.* **2012**, *710*, 641–658. [CrossRef]
15. Civan, F. Effective Correlation of Apparent Gas Permeability in Tight Porous Media. *Transp. Porous Media* **2010**, *82*, 375–384. [CrossRef]
16. Cao, P.; Liu, J.; Leong, Y.K. A Fully Coupled Multiscale Shale Deformation-Gas Transport Model for the Evaluation of Shale Gas Extraction. *Fuel* **2016**, *178*, 103–117. [CrossRef]
17. Yuan, Y.; Gholizadeh, N.; Rahman, S. An Analytical Model of Apparent Gas Permeability for Tight Porous Media. *Transp. Porous Media* **2016**, *111*, 193–214. [CrossRef]
18. Sheng, M.; Li, G.; Tian, S.; Huang, Z.; Chen, L. A Fractal Permeability Model for Shale Matrix with Multi-Scale Porous Structure. *Fractals* **2016**, *24*, 1650002. [CrossRef]
19. Yang, Z.; Wang, W.; Dong, M.; Wang, J.; Li, Y.; Gong, H.; Sang, Q. A Model of Dynamic Adsorption–Diffusion for Modeling Gas Transport and Storage in Shale. *Fuel* **2016**, *173*, 115–128. [CrossRef]
20. Gu, W.; Cheng, Q.; Xu, D.; Yao, S.; Li, H. Investigation of the Gas Pressure Field and Production Rate for Two Typical Proppants: Small-Sized Continuous and Large-Sized Discontinuous Proppants. *Appl. Sci.* **2023**, *13*, 12040. [CrossRef]
21. Geiger, G.H.; Poirier, D.R. *Transport Phenomena in Metallurgy*; Addison-Wesley Publishing Company: Boston, MA, USA, 1973; pp. 36–542.
22. Coutry, S.; Tantawy, M.; Fadel, S. Assessing the Accuracy of Empirical Decline Curve Techniques for Forecasting Production in Unconventional Reservoirs: A Case Study of Haynesville, Marcellus, and Marcellus Upper Shale. *J. Eng. Appl. Sci.* **2023**, *70*, 69. [CrossRef]
23. Shabib-Asl, A.; Plaksina, T. Selection of Decline Curve Analysis Model Using Akaike Information Criterion for Unconventional Reservoirs. *J. Pet. Sci. Eng.* **2019**, *182*, 106327. [CrossRef]